PFG 2014 / 4, 0287 – 0298
Stuttgart, August 2014

Report

Evaluation of a Light-weight Lidar and a Photogrammetric System for Unmanned Airborne Mapping Applications

Gianpaolo Conte, Piotr Rudol & Patrick Doherty, Linköping, Sweden

Keywords: UAS, lidar, sensor fusion, photogrammetry

Summary: This paper presents a comparison of two light-weight and low-cost airborne mapping systems. One is based on a lidar technology and the other on a video camera. The airborne lidar system consists of a high-precision global navigation satellite system (GNSS) receiver, a microelectromechanical system (MEMS) inertial measurement unit, a magnetic compass and a low-cost lidar scanner. The vision system is based on a consumer grade video camera. A commercial photogrammetric software package is used to process the acquired images and generate a digital surface model. The two systems are described and compared in terms of hardware requirements and data processing. The systems are also tested and compared with respect to their application on board of an unmanned aerial vehicle (UAV). An evaluation of the accuracy of the two systems is presented. Additionally, the multi-echo capability of the lidar sensor is evaluated in a test site covered with dense vegetation. The lidar and the camera systems were mounted and tested on-board an industrial unmanned helicopter with maximum take-off weight of around 100 kilograms. The presented results are based on real flight-test data.

Zusammenfassung: *Bewertung eines Lidarsystems mit geringem Gewicht und eines photogrammetrischen Systems für Anwendungen auf einem UAV.* Dieser Beitrag präsentiert einen Vergleich von zwei leichten und kostengünstigen luftgestützten Kartiersystemen. Eines der Systeme basiert auf Laserscanner-Technologie, während das andere eine Videokamera benutzt. Das luftgestützte Laserscannersystem besteht aus einem hochgenauen Empfänger für globale Navigationssatellitensysteme (GNSS), einer inertialen Messeinheit (IMU) auf Basis eines mikro-elektromechanischen Systems (MEMS), einem magnetischen Kompass und einem kostengünstigen Laserscanner. Das optische System basiert auf einer handelsüblichen Videokamera. Ein kommerzielles photogrammetrisches Softwarepaket wird verwendet, um die damit aufgenommenen Bilder zu prozessieren und digitale Oberflächenmodelle abzuleiten. Die beiden Systeme werden beschrieben und in Hinblick auf ihre Anforderungen an Hardware und Datenprozessierung verglichen. Außerdem werden sie in Hinblick auf ihre Eigenschaften bei der Verwendung auf unbemannten Flugkörpern (UAV) getestet und verglichen. Die Genauigkeit beider Systeme wird evaluiert. Zusätzlich wird die Fähigkeit des Laserscanner-Sensors in Hinblick auf Mehrfachechos in einem Testgebiet mit dichter Vegetation untersucht. Beide Systeme wurden auf einem unbemannten Industrie-Helikopter mit einem maximalen Startgewicht von ca. 100 kg montiert. Alle hier präsentierten Daten beruhen auf tatsächlich im Zuge von Testflügen aufgenommenen Daten.

1 Introduction

The work presented in this article focuses on the evaluation of two different traditional technologies for building digital surface models: airborne lidar and photogrammetry. The investigation is done in the context of the newly emerging technology of light-weight unmanned aerial systems (UAS). UAS's offer many advantages over manned aircraft

www.schweizerbart.de
DOI: 10.1127/1432-8364/2014/0200 1432-8364/14/0200 $ 3.00

mainly due to the reduced operational costs. Additionally, UAS's can operate in hazardous environments or during natural catastrophes without endangering the lives of human pilots.

Applying traditional technologies used on full-size manned aircraft to small UAS platforms (below 100 kg take-off weight) is not straightforward as the weight and costs become of main concern. The use of low-cost sensors degrades the system performance but often the cost/benefit balance is still convenient.

Airborne lidar scanner (ALS) systems have been an active research area in recent years. Since their introduction in the mid-90s the technology has developed substantially in terms of increased accuracy, increased pulse repetition rate, introduction of multiple returns (including full waveform digitizing) and integration with a higher accuracy GNSS and inertial navigation systems.

This paper presents a low-cost and light-weight ALS system for close range airborne applications. Additionally, an investigation of the multi-echo capability of the ALS in the context of vegetation measurement is provided. The ALS system is compared to a light-weight vision-based mapping system installed on the same platform.

The paper has the character of a comparative study of the two different mapping modalities. Both systems are light-weight and low-cost and are suitable for installation on a small UAV platform. The main goal of the paper is to compare the systems with regard to the weight, costs, processing requirements and deployment effort.

Due to their different nature, the two systems could be used in a complementary manner in order to compensate their respective weaknesses. For instance, the vision-based system does not work well in featureless environments while the lidar system does not require such features to work properly. On the other hand, lidar systems are difficult to calibrate while vision-based systems are relatively easy in this respect. A combination of a lidar and a vision system could help in the lidar calibration process. In this article the two systems operate independently and a fusion of the two methods will be addressed in a future work.

The ALS and vision-based systems described have been integrated and tested on a Yamaha RMAX helicopter (Fig. 1).

Fig. 1: The UAS Tech Lab RMAX helicopter.

2 Related Work

Using lidar systems on unmanned rotorcraft opens a wide range of applications, but at the same time this poses a number of challenges which have to be addressed. The complications become more severe for medium and small size platforms using low cost sensors. One complication involves the high vibration levels occurring during flight. Additionally, the fidelity of sensors, which are required to be of low weight, is often sacrificed. These problems open a number of research issues which have been addressed in recent years.

A mobile laser scanning system for post-mission map generation from raw data recorded by a suite of sensors consisting of a GNSS receiver, an inertial measurement unit (IMU), and a laser scanner, was presented by Glennie et al. (2013). The system is comparable to our approach, however, it is mainly tailored to be operated from a backpack or a balloon where it achieves a vertical accuracy of up to 3 cm and a horizontal accuracy of 17 cm. A laser mapping system for small helicopters has been developed by Lin et al. (2011). The authors demonstrated the feasibility of their approach by processing data collected during a manual flight.

Mapping using image based solutions have also received a considerable amount of attention in recent years. A set of applications using UAVs equipped with cameras for these purposes are presented in Remondino et al. (2011).

A system composed of a video camera, a laser range finder, GPS and IMU sensors was presented by Nagai et al. (2009). The system includes a new method for direct georeferencing by the combination of bundle block adjustment and Kalman filtering. It allows for objects to be rendered richly in shape and with detailed textures automatically using a UAV flying at a low altitude. The average error of the digital surface model is reported to be approximately 10 cm to 30 cm. In contrast with our work, where low-cost MEMS inertial sensors are used, they use fiber-optic gyroscopes which are several orders of magnitude more accurate and expensive.

As previously stated, lidar systems used on helicopters experience a high level of vibrations during flight. Consequently, range measurements depending on pose estimations are typically erroneous and conventional methods for point cloud registration might fail in certain cases. Kaestner et al. (2006) proposed a probabilistic approach for alignment and change detection using range sensor data and a non-rigid point cloud registration that implicitly deals with high estimation errors. The system was evaluated on a helicopter platform.

A comparison between digital elevation models of a cultural heritage site generated using a camera equipped rotorcraft UAV and a terrestrial laser scanner can be found in Eisenbeiss & Zhang (2006). The results presented show the difference mean value to be less than 1 cm with a standard deviation of 6 cm.

Lidar systems have also been extensively used for forestry applications in order to estimate key forest structure characteristics such as canopy height, topography, average stem diameter, canopy volume etc. Examples of such systems can be found in Pirotti (2011) and Wallace et al. (2012). In particular the former investigates the use of full waveform lidar (FWL) technology. In contrast to traditional discrete return lidar, FWL samples the entire back-scattered signal intensity at high rate allowing for an in-depth study of vegetation parameters. However, this technology is still quite complex and expensive and at the moment not suitable for experimentation on small UAV platforms.

The rich body of literature in this field shows the existence of similar lidar-based and vision-based systems as the one presented in this paper. However, proper evaluations and comparisons of these techniques when used in the same context, i.e. the same flying platform, same environmental conditions, the same flight plan, are not common. This is especially true in the new domain of small size and low-weight unmanned aircraft where the sensor technology used is several orders of magnitude less expensive. This article is intended to be a contribution in this context.

3 Helicopter Platform

In this paper, the platform used for experimentation is the UAS Tech Lab (UASTL) RMAX. It is a modified Yamaha RMAX helicopter (Fig. 1). It uses a 21 hp two-strokes gas engine with an empty weight of 61 kg and a maximum take-off weight of 95 kg. The main rotor diameter is 3.1 m. The UASTL RMAX is capable of autonomous flight from take-off to landing. The hardware and software enabling the autonomous flight capabilities were developed at the Division of Artificial Intelligence and Integrated Computer System (AIICS) at Linköping University (Doherty et al. 2004, Conte 2009).

4 Airborne Lidar System Description

The following subsections describe the hardware components and algorithms used in the proposed airborne lidar system.

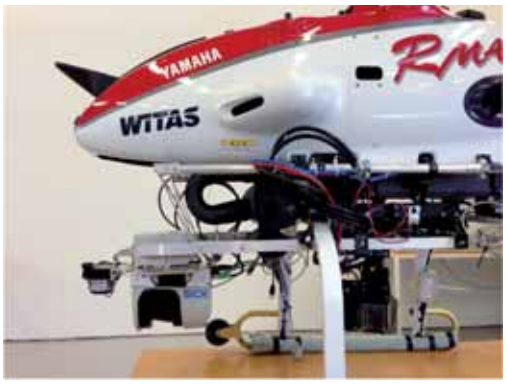

Fig. 2: The airborne lidar and camera systems mounted on the UASTL RMAX helicopter.

4.1 *Hardware*

The ALS described in this paper is depicted in Fig. 2. The system consists of a class 1 SICK LMS511 PRO lidar with multi-echoes capability. The laser wave length is 905 nm and the maximum scanning angle is 190º with a maximum angular resolution of 0.166º. The beam divergence is 11 mrad which gives a spot size of about 50 cm at a distance of 45 m, i.e. a typical flight altitude of the experiments performed here. Other characteristics of the scanner are reported in Tab 1.

The GNSS positioning system used is the Javad TRE-G3T. It is capable of tracking GPS (L1/L2/L2C/L5), GLONASS (L1/L2) and Galileo (E1/E5A) satellite systems. The ground reference correction signal is transmitted to the on-board receiver using the Telit TinyOne Plus 868 MHz wireless datalink. An Analog Devices ADIS16375 MEMS inertial measurement unit (IMU) and a Honeywell HMR3000 magnetic compass are additional parts of the system (see Tab. 1 for technical specifications). An embedded PC104 1.6 GHz Intel Atom computer is used for on-board data acquisition. The schematic of the system is presented in Fig. 3. The picture also includes the camera system for photogrammetric reconstruction described in section 5.

The lidar and the IMU sensors are mounted on a vibration isolated rig in front of the UASTL RMAX platform (see Fig. 2). The data acquisition PC and the GNSS receiver are mounted on a vibration isolated plate on a side of the helicopter. The magnetic compass is placed on the helicopter tail boom to minimize magnetic interferences influencing the measurements.

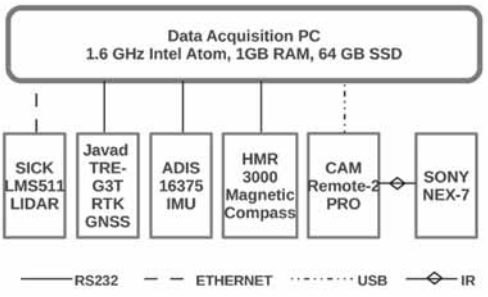

Fig. 3: Schematics of the ALS and photogrammetric hardware components (SSD = solid state drive, SICK = manufacturer of sensors, LMS = laser measurement sensor, TRE-G3T = GNSS-board, ADIS = Analog Devices (company), HMR = Honeywell digital compass, Sony NEX-7 = camera).

Compared to high-end ALSs traditionally used in the remote sensing field, the system presented here has a much lower cost, approximately 15,000 Euro versus 200,000 Euro for high-end systems. Additionally, it is lighter but has lower range and accuracy. The accuracy problem must be placed in the context of the intended usage of the system. The target use for the proposed ALS is for small and medium sized UASs flying at low altitudes of 50 m – 100 m above ground level (AGL). Typically, high-end ALS's installed on manned aircraft operate at altitudes of 500 m AGL or more. Considering that direct georeferencing errors increase with the AGL altitude it can be

Tab. 1: Airborne lidar system sensor specification.

SICK Laser LMS511 PRO				
Data Rate	Range	Range err.	Weight	Cost
28.6 kHz	80 m	1.8 cm 1σ	3.7 kg	6000 €
Javad GNSS TRE-G3T, AirAnt antenna				
Data Rate	Pos. Err.	RTK	Weight	Cost
20 Hz	5 cm	yes	77 g 320 g (antenna)	6500 €
MEMS IMU ADIS16375				
Data Rate	Gyro bias	Acc. bias	Weight	Cost
100 Hz	12°/hr	0.13 mg	25 g	450 €
Compass HMR3000				
Data Rate	Accuracy	Resolution	Weight	Cost
15 Hz	<1.5°	0.1°	92 g	600 €
On-board Data Acquisition PC104				
Processor	Memory	Mass storage	Weight	Cost
Atom 1.6 GHz	2 GB SDRAM	SSD 100 Gb	400 g	900 €
		Tot.	4.6 kg	14450 €

reasonable to assume that, from an accuracy point of view, low cost ALS flying at low altitudes can be compared to high-end ALS flying at higher altitudes. Insights on direct georeferencing methods can be found in Skaloud (1999).

4.2 *Lidar System Calibration*

Calibration of sensors is essential to reduce the systematic errors in the system. In case of ALS, a calibration procedure aims at computing the boresight parameters, i.e the mounting angle between an IMU and a lidar scanner, the lever arms between a lidar, an IMU and a GNSS antenna and biases in the lidar scanner device (ranges and mirror angle).

ALS calibration has been an active area of research and it is still the case that a standard procedure has not yet been defined. An analytical and automatic procedure which estimates all the calibration parameters is difficult to apply because of the correlation between the parameters. Another problem lies in the difficulty of extracting features out of a lidar point cloud. Bang (2010) includes a review of several different approaches developed for ALS calibration. Professional ALSs are still calibrated through empirical ad-hoc procedures requiring well defined features such as planar patches or edges.

An empirical lab calibration was performed for this work. Lever arms between the IMU, the lidar and the GNSS antenna were directly measured on the platform and the correction added in the software. Boresight estimation between IMU and lidar was performed by acquiring IMU and lidar data (the IMU is rigidly mounted on the lidar) while manually pitching and rolling the scanner unit. A point cloud was generated from the acquired data and a visual assessment of the distortion of known features, e.g. walls, floor and ceiling, indicates whether a boresight correction was needed. The boresight parameters were empirically adjusted until such distortion was judged acceptable. However, no numerical criteria was applied but engineering judgment after visual inspection of the point cloud.

4.3 *Data Acquisition*

The raw data produced by the sensors described in the previous section is saved by the data acquisition PC on a solid state drive (SSD) during a flight. The software developed for the purpose of this work collects data using the appropriate interfaces (see Fig. 3) and saves it in text files. The time-stamping of data is done at the time of receiving them by the acquisition PC which reads the sensors at a high-rate. Hardware triggering of sensors is not used and the time of acquisition and transfer has proven to be negligible for the intended application. However, in order to improve the data synchronization a method for hardware triggering can be used as described by Wehr & Lohr (1999). Even though a non-realtime Linux OS is used, no negative consequences of it have been observed during the system evaluation and operation.

4.4 *Processing*

The data processing workflow includes: (a) synchronized data collection during a flight; (b) post-processing of the IMU, RTK GNSS and compass data using an efficient two-pass smoothing algorithm; (c) direct georeferencing of lidar measurements and point cloud generation.

Smoothing techniques are used to reconstruct an optimal state solution using past, current and future measurements. The algorithm used here is the Rauch-Tung-Striebel smoother (RTSS) as presented in Rauch et al. (1965). It belongs to the fixed-interval smoother class. The whole dataset was used to compute the smoothed trajectory.

The smoothing algorithm is implemented in forward and backward processing parts. The forward part is a 15-state extended Kalman filter (EKF). The state vector includes positions, velocities, attitudes, accelerometers and gyroscope biases. The EKF is implemented in a loosely coupled scheme using the error dynamic formulation where the navigation errors of the inertial navigation system (INS) are estimated and used to correct the navigation solution (Shin 2005). The measurement update step is realized using the so-called UD

algorithm (Bierman 1977) and is executed at 20 Hz rate (GNSS update rate). The filter time update is performed at the rate of 100 Hz, which is the same as the IMU data rate.

The backward part is implemented with the RTSS recursive algorithm described in Brown & Hwang (1992), p. 334. The advantage of the RTSS algorithm is that its implementation is of low complexity compared to other smoothing algorithms. On the other hand, it requires a certain amount of memory storage since some of the parameters must be retained during the forward pass at each time step.

5 Vision-based System Description

This section describes the photogrammetric hardware and software components used in this paper.

5.1 *Hardware*

The camera used in the photogrammetric system is a Sony Nex-7 and it is mounted, pointing downward, on the same vibration isolated rig used for the lidar in front of the UASTL RMAX platform (see Fig. 2). The imaging sensor size is 23.5 × 15.6 mm² (APS-C size), with a total of 24 megapixels and is based on the CMOS technology. The camera features a mirror-less construction and allows for changing lenses. It has been equipped with a fixed focal length lens as it guarantees better optical parameter stability during flight. The lens chosen has a 16 mm focal length (or 24 mm if using the 35 mm equivalent terminology) with the angle of view of 83º. The total weight of the camera is 423 grams. The communication between the camera and the data acquisition PC is realized using the CAMremote-2 PRO (http://vp-systems.eu/camremote.html) infrared interface. The interface is used only for triggering the image acquisition. The physical connection is shown schematically in Fig. 3.

5.2 *Camera System Calibration*

The image processing software described in more detail in section 5.4 estimates the camera internal parameters during the processing of the images. Therefore, there is no need for an explicit calibration procedure. This is a great advantage compared to the complex calibration procedure required for the ALS. The software estimates the lens focal length, the principal point, radial and tangential lens distortion parameters. It is important that these parameters remain stable during flight. This is usually not the case for cheap consumer cameras. In this application, a fixed focal length lens is used in order to maintain a sufficient optical stability.

5.3 *Data Acquisition*

Particular care must be taken in the flight planning phase to ensure that the pictures collected have sufficiently large overlapping regions. More information about flight plans is provided in section 6. The time of triggering of the image capture is logged and used for synchronization with the GNSS data. Images are saved on the camera's memory card and downloaded after a flight for processing.

5.4 *Processing*

As already mentioned, the processing is done using *Pix4UAV Desktop 3D 2.1* (Pix4d 2013) software from Pix4D company. It uses a structure-from-motion approach and implements the complete workflow in an automated way. The workflow can be divided into 3 main steps. The first step consists of keypoint extraction using SIFT (Lowe 2004), keypoint matching, camera calibration and pose optimization using bundle block adjustment and finally point cloud geolocation using GNSS geotags or ground control points. In the second step, a point cloud densification and filtering is performed. The last step includes a DSM (digital surface model) generation, image ortho-rectification and orthomosaic blending. At the end of the first step the software produces a report containing information about the quality of the acquired images. Based on the reported results the user can decide to continue with the processing or to repeat the image acquisition.

The software allows use of either ground control points or geo-tagged images. The second option was used in this work as the GNSS position is already available and used for the lidar system. Image geo-tagging information is added in the exchangeable image file (EXIF) metadata. Images are geo-tagged using latitude, longitude and altitude information taken from the on-board GNSS.

Pix4D is similar to many other software packages like PhotoScan, MicMac, Bundler, etc. A description of alternative software solutions can be found in Neitzel & Klonowski (2011). In this article the authors do not make any comparative statements between Pix4D and other solutions because of lack of experience in using other photogrammetric software. Pix4D software was chosen as a representative example of an image-based DSM solution for comparison with the proposed ALS system.

6 Experimental Results

This section presents surface reconstruction results for two different landscapes: a small airfield with a few building structures and a tree covered area. The reconstruction of the airfield is performed using the ALS and photogrammetric system presented in previous sections. Photogrammetric reconstruction of the tree-covered field is not reported here as this technique presents additional complications in this kind of environment.

6.1 *Airfield Mapping*

The object of this study is an airfield located near Motala (Sweden). An overview of the area is depicted in Fig. 4. The size of the mapped area is about 1.6 ha. The flight was performed using a rectangular scanning pattern consisting of 3 flight lines as shown in Fig. 4. The flight parameters (velocity, altitude, distance between scanning lines) were chosen in order to satisfy the requirements of both the ALS and the vision-based systems. Lidar and camera images were acquired simultaneously.

The first parameter chosen was the flight altitude above the ground (about 45 m). The value was chosen in order to operate far enough from the lidar range limit (about 80 m). Given the flight altitude, the other parameters were chosen in order to satisfy the constraints imposed by the vision system. In order to reach a satisfactory accuracy, the Pix4D software requires a number of keypoint matches greater than 1000 per image pair. This is usually achieved when the image front overlap is greater than 75% and the image side overlap is greater that 40% on an easy terrain, i.e. rich in features such as urban terrain, for instance. In order to satisfy such requirements the flight speed was set at 3 m/s with a distance of 40 m between consecutive flight lines. A wide angle camera lens was also used (16 mm as described in section 5.1). Additionally, the image acquisition rate was set at 1 image every 2 seconds. The camera image size was set to 3008 × 2000 pixels resulting in a ground sampling distance (GSD) of about 2.5 cm/pixel. The lidar scanning rate was set at the maximum speed of 100 Hz with a scanning angular resolution of 0.66° resulting in a point density of 50 points/m^2. This is a much larger number compared to the typical point density obtained from an ALS used on manned airborne plat-

Fig. 4: Orthomosaic of the airfield near Motala (Sweden). The yellow lines show the scanning pattern used to cover the area starting from point a to f.

forms (below 10 pts/m^2). The scanning angle was set at 50°.

Fig. 5 (a) shows a snapshot of the airfield surface model generated with the ALS. The photogrammetric model displayed in Fig. 5 (b) was generated from 76 images.

From a visual inspection of Fig. 5 (a) and (b) it can be observed that neither the ALS nor the photogrammetric models are complete. Some parts of the buildings are missing in both models. It can be observed also that the photogrammetric model is slightly more noisy than the ALS one. In addition, on the right side of the photogrammetric model there is a certain amount of erroneous elevation (which is not present in reality) and the trees are not modeled properly. The reason could be an insufficient image overlap since some parts of the area have a poor feature content.

In order to give an indication about the accuracy of the different point clouds generated, it was decided to accurately model the long hangar building (at the bottom of Fig. 4). The resulting model has been used as the best available reference. The following procedure was used in order to build the reference model.

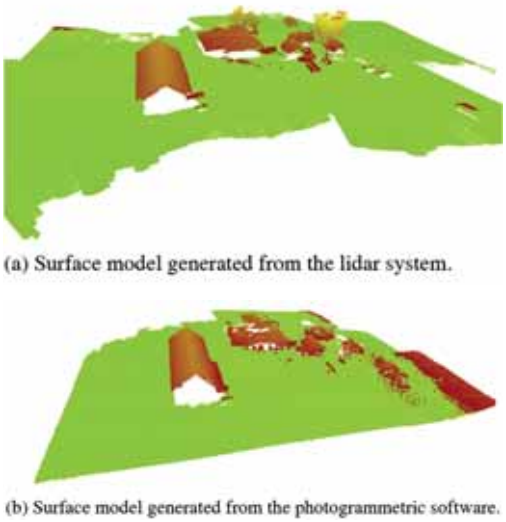

Fig. 5: Digital surface model of the airfield. The green colour represents the ground surface. An elevation value greater than 20 cm (the elevation is intended from the ground surface which is substantially flat) is represented in red colour. The red becomes lighter with an increase in elevation.

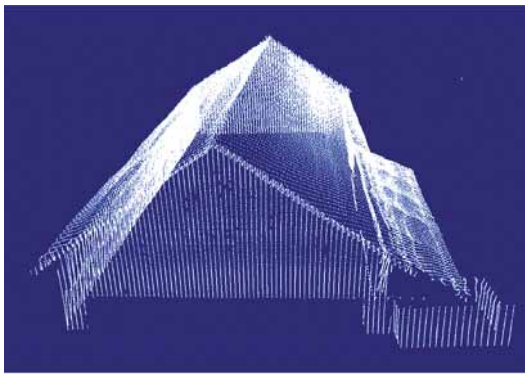

Fig. 6: Hangar reference model generated from lidar measurements taken from the ground.

The four building façades were reconstructed from lidar measurements taken from 4 different positions on the ground and at a distance of around 30 m from each façade. Each façade was scanned by changing the lidar elevation angle while keeping the position static. The resulting point cloud of the hangar was accurately geolocated by measuring the four hangar corners with the same RTK GNSS system used on the helicopter. A 30 s static measurement acquisition for each corner was performed and the mean value was taken for each corner. The lidar scanner used for the model construction was the same as that installed on the helicopter. Given the accuracy of the sensors used (see Tab. 1) we believe that the accuracy of the resulting reference model is of the order of 5 cm. The model is shown in Fig. 6.

The hangar roof was captured from each of the 3 lidar strips generated from the scanning segments *a–b*, *c–d*, *e–f* (Fig. 4). Each of the roof reconstructions were compared to the reference model while only one photogrammetric hangar roof reconstruction was available for comparison. The error statistic of the different point clouds have been computed using CloudCompare software (CLOUDCOMPARE 2013) and are reported in Tab. 2. The CloudCompare *cloud-to-cloud* distance command has been used. The mean error generated by the lidar system has a strong fluctuation depending on the scanning direction. This is potentially due to the use of a magnetic compass which introduces a relatively large error in heading estimation and/or an insufficient sensor calibration. The standard deviation is more

consistent between the different lidar scans. It can be observed that the third scan (*e–f*) has a higher standard deviation value compared to the first two. This is expected due to the higher angular incidence of the lidar beams with the hangar roof increasing the effects of the attitude errors.

A visualization of the point cloud noise of the two reconstruction methods is depicted in Fig. 7. The lidar and photogrammetric point clouds have been registered with the reference model using the iterative closest point (ICP) method (Besl & McKay 1992) to remove the mean distance. It can be noticed that the lidar point cloud is slightly less noisy than the photogrammetric one (σ is smaller) but it has stronger systematic deviations.

For the lidar system, the dominating error source comes from the MEMS IMU and the magnetic compass. From the type of IMU used the expected pitch and roll estimation errors are in the order of 0.2º – 0.3º. With a ground altitude of 45 m this leads to a lidar survey horizontal error of 15 cm – 25 cm. The vertical error is directly related to the RTK GNSS vertical accuracy and the lidar scanner range accuracy (both in the sub-decimetre accuracy range). The other expected relevant source of error comes from heading estimation. The magnetic compass accuracy is in the order of 1º – 1.5º. At a ground altitude of 45 m and scanning angle of 50º, a horizontal error of 35 cm – 55 cm at the border of the lidar strip is expected. The use of a double GNSS antenna instead of a magnetic compass for heading estimation can reduce the heading error of one order of magnitude.

For the photogrammetric system, given the flight altitude H = 45 m, the height/base ratio H/B = 4 (where B is the baseline between consecutive images), the camera focal length f = 16 mm and the standard deviation of a measured image coordinate σ_p = 0.0077 mm, the expected photogrammetric accuracy is $\sigma_{xy} \approx$ 2 cm (horizontal) and $\sigma_z \approx 9$ cm (vertical).

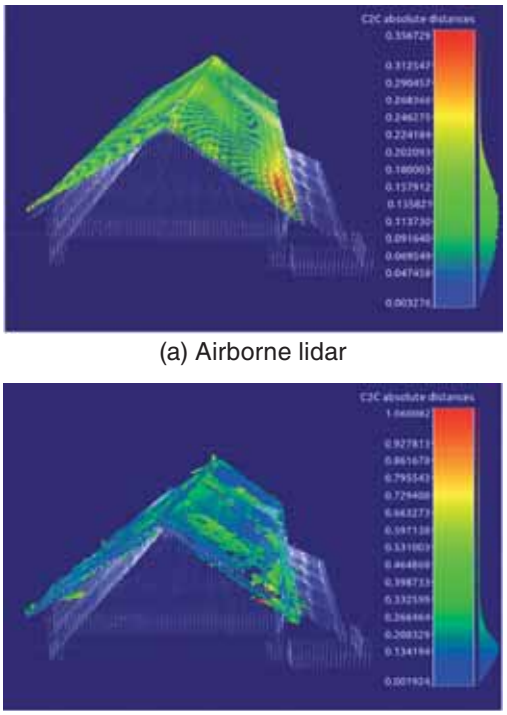

(a) Airborne lidar

(b) Photogrammetry

Fig. 7: Deviation between the reference model and reconstruction based on the two methods examined. The values of on the colour bars are in meters.

6.2 *Multi-echo Capabilities*

The aim of this section is to evaluate the performance of the multi-echo capability of the lidar sensor when operating over a forest. Valuable information such as canopy height could

Tab. 2: Point cloud error statistics in meters. Mean is the mean error, σ is the standard deviation and *rms* is the RMS error of the distances between the point clouds.

Lidar a–b	Lidar c–d	Lidar e–f	Photogrammetry
mean: 0.005	mean: 0.607	mean: 0.263	mean: 0.080
σ: 0.112	σ: 0.107	σ: 0.139	σ: 0.148
rms: 0.112	rms: 0.616	rms: 0.297	rms: 0.168

be extracted from lidar measurements. The capability of recording 5 different echoes for one pulse can improve the performance in estimating the canopy height compared to a single return lidar sensor.

For this purpose a flight-test was performed over a small forest with the canopy height of about 25 m. The flight altitude was approximately 50 m from the ground level. All five lidar echoes were recorded in the log file. The flight path was executed at the forest border. Measurements falling outside the forest area were manually removed. Fig. 8 (a) shows a snapshot of the helicopter camera view over the forest. Fig. 8 (b) shows a side view snapshot of the lidar measurements while in Fig. 8 (c) only the ground-points are displayed. The ground-points are extracted from elevation by thresholding using the flat-ground assumption.

Tab. 3 presents statistics of the pulse returns of the scanned area. As can be observed from the data, the 4th and 5th echoes did not provide any useful information due to the low number of returns. This implies that the multi-echo capability of this sensor does not provide additional bare earth information in this kind of environment.

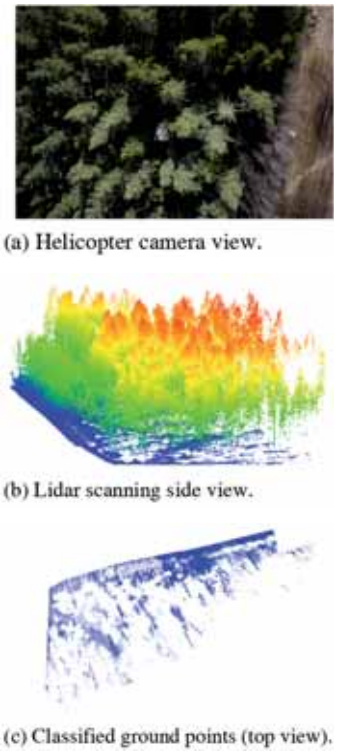

(a) Helicopter camera view.

(b) Lidar scanning side view.

(c) Classified ground points (top view).

Fig. 8: Camera image and lidar measurements.

Tab. 3: Number of echoes and classified groundpoints for the scanned forest area of 1 ha size.

Echoes	Total	Ground	% Ground
1st	1141195	182361	16%
2nd	172507	27502	16%
3rd	10233	1571	15.3%
4th	241	18	7.47%
5th	3	3	100%
all	1324179	211455	16%

7 Conclusions

The paper presented two systems for building digital surface models: an airborne lidar system and photogrammetry-based vision system.

The analysis presented shows that the ALS errors are in line with the expectations. The major source of errors come from the low-cost IMU and the magnetic compass. A dual GNSS antenna can reduce the heading error leading to a more accurate DSM. An in-flight lidar boresight calibration procedure could further reduce the reconstruction errors.

Vision-based techniques can achieve centimetre level accuracy with a simpler system without dealing explicitly with complex calibration and synchronization issues. The flight planning for a photogrammetric system is more complex compared to the ALS system as it is subjected to constraints on the image overlap. Areas with poor visual content have been problematic for the vision system during the tests while the lidar has not shown any problem in this respect.

The ALS hardware is substantially heavier than the video camera, 4.6 kg compared to 0.9 kg (the camera including the GNSS receiver). The cost of the ALS presented is about 15,000 Euro while the camera used was around 1,000 Euro including the lens. It should be pointed out that if an accurate geolocation

of the DSM is required, an RTK GNSS system must be included with the camera system increasing the costs up to 8,000 – 9,000 Euro.

Acknowledgements

This work is partially supported by the EU FP7 project SHERPA (grant agreement 600958), the Swedish Research Council (VR) Linnaeus Center for Control, Autonomy, and Decision-making in Complex Systems (CADICS), the ELLIIT network organization for Information and Communication Technology, the Swedish National Aviation Engineering Research Program NFFP6 and the SSF – the Swedish Foundation for Strategic Research (CUAS Project).

References

Bang, K.I., 2010: Alternative Methodologies for LiDAR System Calibration. – PhD thesis, Schulich School of Engineering, University of Calgary, AL, Canada.

Besl, P. & McKay, N.D., 1992: A Method for Registration of 3-D Shapes. – Pattern Analysis and Machine Intelligence, IEEE Transactions on **14** (2): 239–256.

Bierman, G., 1977: Factorization Methods for Discrete Sequential Estimation. – Academic Press, New York, NY, USA.

Brown, R. & Hwang, P., 1992: Introduction to Random Signal and Applied Kalman Filtering. – John Wiley & Sons, Inc., second edition.

Cloudcompare, 2013: (version 2.4) [GPL software]: http://www.danielgm.net/cc/ (25.4.2014).

Conte, G., 2009: Vision-Based Localization and Guidance for Unmanned Aerial Vehicles. – PhD thesis, Linköping University, Sweden.

Doherty, P., Haslum, P., Heintz, F., Merz, T., Nyblom, P., Persson, T. & Wingman, B., 2007: A Distributed Architecture for Autonomous Unmanned Aerial Vehicle Experimentation. – Distributed Autonomous Robotic Systems **6:** 233–242.

Eisenbeiss, H. & Zhang, L., 2006: Comparison of DSMs Generated from Mini UAV Imagery and Terrestrial Laser scanner in a Cultural Heritage Application. – ISPRS International Archives of Photogrammetry, Remote Sensing and Spatial Information Sciences **XXXVI** (part 5).

Glennie, C., Brooks, B., Ericksen, T., Hauser, D., Hudnut, K., Foster, J. & Avery, J., 2013: Compact Multipurpose Mobile Laser Scanning System – Initial Tests and Results. – Remote Sensing **5** (2): 521–538.

Kaestner, R., Thrun, S., Montemerlo, M. & Whalley, M., 2006: A Non-rigid Approach to Scan Alignment and Change Detection Using Range Sensor Data. – Field and Service Robotics **25** (4): 179–194, Springer, Berlin, Heidelberg.

Lin, Y., Hyyppä, J. & Jaakkola, A., 2011: Mini-UAV-borne LIDAR for Fine-scale Mapping. – IEEE Geoscience and Remote Sensing Letters **8** (3): 426–430.

Lowe, D., 2004: Distinctive Image Features from Scale-invariant Keypoints. – International Journal of Computer Vision **60:** 91–110.

Nagai, M., Chen, T., Shibasaki, R., Kumagai, H. & Ahmed, A., 2009: UAV-borne 3-D Mapping System by Multisensor Integration. – IEEE Transactions on Geoscience and Remote Sensing **47** (3): 701–708.

Neitzel, F. & Klonowski, J., 2011: Mobile 3d Mapping with a Low-cost UAV System. – ISPRS International Archives of the Photogrammetry, Remote Sensing and Spatial Information Sciences **XXXVIII-1/C22**.

Pirotti, F., 2011: Analysis of Full-waveform Lidar Data for Forestry Applications: A Review of Investigations and Methods. – iForest – Biogeosciences and Forestry **4:** 100–106.

Pix4d, 2013: Pix4uav desktop 3D (version 2.1): http://pix4d.com/ (25.4.2014).

Rauch, H., Tung, F. & Striebel, C., 1965: Maximum Likelihood Estimates of Linear Dynamic Systems. – AIAA Journal **3** (8): 1445–1450.

Remondino, F., Barazzetti, L., Nex, F., Scaioni, M. & Sarazzi, D., 2011: UAV Photogrammetry for Mapping and 3D Modeling – Current Status and Future Perspectives. – ISPRS International Archives of the Photogrammetry, Remote Sensing and Spatial Information Sciences **XXXVIII-1/C22:** 25–31.

Shin, E.-H., 2005: Estimation Techniques for Low-Cost Inertial Navigation. – PhD thesis, University of Calgary, AL, Canada.

Skaloud, J., 1999: Optimizing Georeferencing of Airborne Survey Systems by INS/DGPS. – PhD thesis, University of Calgary, AL, Canada.

Wallace, L., Lucieer, A., Watson, C. & Turner, D., 2012: Development of a UAV-Lidar System with Application to Forest Inventory. – Remote Sensing **4** (6): 1519–1543.

Wehr, A. & Lohr, U., 1999: Airborne Laser Scanning: An Introduction and Overview. – ISPRS Journal of Photogrammetry and Remote Sensing **54** (2-3): 68–82.

Address of the Authors:

Dr. Gianpaolo Conte, M.Sc. Piotr Rudol & Prof. Patrick Doherty, Linköping University, Department of Computer and Information Science, S-581 83 Linköping, Sweden, Tel.: +46-13-28-1167, -1606, -2426, e-mail: {gianpaolo.conte}{piotr.rudol}{patrick.doherty}@liu.se

Manuskript eingereicht: Oktober 2013
Angenommen: April 2014